Advanced Glycation End Product (AGE) Accumulation on Bruch's Membrane: Links to Age-Related RPE Dysfunction

Josephine V. Glenn,[1] Helen Mahaffy,[1] Keqiang Wu,[2] Gill Smith,[2] Ryoji Nagai,[3] David A. C. Simpson,[1] Michael E. Boulton,[2,4] and Alan W. Stitt[1]

Purpose. Advanced glycation end products (AGEs) accumulate during aging and have been observed in postmortem eyes within the retinal pigment epithelium (RPE), Bruch's membrane, and subcellular deposits (drusen). AGEs have been associated with age-related dysfunction of the RPE—in particular with development and progression to age-related macular degeneration (AMD). In the present study the impact of AGEs at the RPE-Bruch's membrane interface was evaluated, to establish how these modifications may contribute to age-related disease.

Methods. AGEs on Bruch's membrane were evaluated using immunohistochemistry. A clinically relevant in vitro model of substrate AGE accumulation was established to mimic Bruch's membrane ageing. Responses of ARPE-19 growing on AGE-modified basement membrane (AGE-BM) for 1 month were investigated by using a microarray approach and validated by quantitative (q)RT-PCR. In addition to identified AGE-related mRNA alterations, lysosomal enzyme activity and lipofuscin accumulation were also studied in ARPE-19 grown on AGE-BM.

Results. Autofluorescent and glycolaldehyde-derived AGEs were observed in clinical specimens on Bruch's membrane and choroidal extracellular matrix. In vitro analysis identified a range of dysregulated mRNAs in ARPE-19 exposed to AGE-BM. Altered ARPE-19 degradative enzyme mRNA expression was observed on exposure to AGE-BM. AGE-BM caused a significant reduction in cathepsin-D activity in ARPE-19 ($P < 0.05$) and an increase in lipofuscin accumulation ($P < 0.01$).

Conclusions. AGEs influence ARPE-19 mRNA expression profiles and may contribute to reduced lysosomal enzyme degradative capacity and enhanced accumulation of lipofuscin. Formation of AGEs on Bruch's membrane may have important consequences for age-related dysfunction of the RPE, perhaps leading to age-related outer retinal disease. (*Invest Ophthalmol Vis Sci.* 2009;50:441–451) DOI:10.1167/iovs.08-1724

Bruch's membrane and the overlying RPE form a dynamic filtration barrier between the dense vascular network of the choriocapillaris and the retinal neuropile. This pentalaminar structure consists of complex layers of extracellular matrix proteins that offer structural support, a scaffold for sequestration of biologically active molecules and sites for dynamic RPE–substrate interactions.[1]

Bruch's membrane displays structural and physiological changes with age, including reconfiguration of chemical composition and an increase in overall thickness.[1,2] Component collagens show decreased solubility and increased cross-linking with age[3]; whereas, in general, there is an age-related accumulation of granular, membranous, filamentous, and vesicular material.[4] A progressive elevation in lipid content in Bruch's membrane also occurs throughout life[5] and an exponential increase in phospholipids, triglycerides, fatty acids, and free cholesterol content of Bruch's membrane has been observed from patients older than 50 years.[6] Such observations are probably linked to the presence of extracellular drusen which indicate the onset of age-related outer retinal disease.[7]

A well-established phenomenon during normal ageing is the modification of proteins by Maillard reactions, leading to so-called advanced glycation end products (AGEs).[8] Formation of these adducts is related to reaction with glucose, lipid peroxidation products or various α-oxaloaldehydes such as methylglyoxal (MGO) and glycolaldehyde (GA).[8] AGEs accumulate especially, but not exclusively, on long-lived structural proteins such as collagens and lens crystallins[9] and are recognized as important instigators of age-related disease by altering macromolecular structure and function.[10] Qualitatively, AGEs are increased in RPE, drusen, and Bruch's membrane from ageing eyes and in patients with age-related macular degeneration (AMD),[11–15] and it has been shown that these adducts also occur in basal lamina deposits from human maculae.[16] AGE formation is associated with age-related chronic inflammation at the outer retina in an in vivo model,[17] and feeding mice high levels of galactose (leading to enhanced AGE-formation) induces age-related defects in Bruch's membrane.[18] Furthermore, a new animal model of AMD has been proposed using glycoxidized (AGE-modified) microspheres to mimic lipofuscin accumulation in the outer retina.[19] In vitro, AGEs can induce various abnormal responses in ARPE-19, including induction of enhanced VEGF expression, a response that may be modulated by the AGE-binding protein galectin-3[20] and the receptor for AGEs (RAGE).[21]

In the present study, we used an in vitro model of RPE (ARPE-19 monolayers) exposed to an AGE-modified basement membrane that has clinical relevance. The effects on ARPE-19 mRNA expression have been assessed by using a microarray approach, followed by determination of how exposure to an

From the [1]Centre for Vision and Vascular Science, School of Medicine, Dentistry and BioMedical Science, Queen's University, Northern Ireland, United Kingdom; the [2]Department of Anatomy and Cell Biology, University of Florida, Gainesville, Florida; the [3]Department of Medical Biochemistry, Graduate School of Medical and Pharmaceutical Sciences, Kumamoto University, Kumamoto, Japan; and the [4]School of Optometry and Visual Sciences, Cardiff University, Cathays, Cardiff, United Kingdom.

Supported by Wellcome Trust Grant 066193/A/01/Z, Action Medical Research, the Medical Research Council (MRC), and a Department for Employment and Learning–Northern Ireland (DEL–NI) PhD studentship.

Submitted for publication January 11, 2008; revised June 2, 2008; accepted October 24, 2008.

Disclosure: **J.V. Glenn**, None; **H. Mahaffy**, None; **K. Wu**, None; **G. Smith**, None; **R. Nagai**, None; **D.A.C. Simpson**, None; **M.E. Boulton**, None; **A.W. Stitt**, None

The publication costs of this article were defrayed in part by page charge payment. This article must therefore be marked "*advertisement*" in accordance with 18 U.S.C. §1734 solely to indicate this fact.

Corresponding author: Alan W. Stitt, Centre for Vision and Vascular Science, School of Medicine, Dentistry and BioMedical Science, Queen's University Belfast, Royal Victoria Hospital, Belfast BT12 6BA, Northern Ireland, UK; a.stitt@qub.ac.uk.

AGE cross-linked substrate influences key aspects of age-related RPE dysfunction. After array outcomes, particular emphasis has been placed on cathepsin-D activity and subsequent lipofuscin accumulation on AGE-exposed cells.

METHODS

AGEs in Bruch's Membrane from Clinical Samples

Human eyes (Bristol Eye Bank/Cardiff University, United Kingdom; $n = 8$) were obtained from donors of various ages (34–89 years) and gender, none of whom had a diagnosis of AMD. The eyes were retrieved approximately 4 hours after death and fixed in 4% (wt/vol) paraformaldehyde (PFA; Sigma-Aldrich Company Ltd., Dorset, UK) for 1 hour at room temperature. All methods were performed in accordance with the tenets of the Declaration of Helsinki for any research involving human tissue. In addition, informed consent was obtained from relatives before the study, and ethical approval was obtained from Research Ethics Committees of all involved Institutions.

After fixation, samples of RPE-Bruch's membrane-choroid adjacent to the macula were paraffin embedded and 5-μm-thick sections cut and placed onto slides. The sections were deparaffinized by washing in xylene three times for 5 minutes each, followed by rehydration in 100% and 95% (vol/vol) ethanol and distilled H_2O. All specimens for immunostaining were permeabilized with phosphate-buffered saline (PBS)-Tween (0.1%) for 20 minutes and then blocked with 5% normal goat serum (NGS) in permeabilization buffer for 20 minutes.

Autofluorescent AGEs were visualized by using a high-resolution confocal spectral imaging system (TCS SPE; Leica Microsystems, Milton Keynes, UK). DAPI staining was used to visualize cell nuclei within 7-μm donor eye sections, prepared as above. The dual lambda (λ) scanning approach allows for emission detection over a wider range (tunable spectral detection, ~400–800 nm) and enabled detection of several different AGEs at their characteristic wavelengths with defined separation. Each different band was then pseudocolored for ease of identification.

GA modifications were detected by using monoclonal antibodies raised against anti-glycolaldehyde-pyridine, which were incubated on the sections overnight at 4°C. Some sections were incubated with PBS alone or murine IgG (DakoCytomation Ltd., Glostrup, Denmark), as negative and isotype controls, respectively. Sections were gently washed in PBS-Tween (five times for five minutes each) before incubation with the appropriate Alexa 488 conjugated secondary antibody (Molecular Probes-Invitrogen, Paisley, UK) for 1 hour at room temperature. They were then washed with PBS-Tween (five times for five minutes each) before mounting in medium containing propidium iodide (PI; Vectashield; Vector Laboratories, Burlingame, CA). The sections were visualized by fluorescence microscopy and recorded using an image analysis system (Lucia GF; Nikon, Surrey, UK).

Cell Culture and Preparation of AGE-Modified Matrix

The human RPE cell line ARPE-19 was obtained from ATCC (Rockville, MD). The cells were maintained as described previously[22]; and on reaching confluence they were maintained in 2% FCS for 1 month after which time, stable, polarized monolayers had formed.

A solubilized substrate rich in common basement membrane (BM) matrix components (Matrigel; BD Biosciences, Oxford, UK) is a suitable substrate to mimic the innermost face of Bruch's membrane. AGE modification of this BM extract (AGE-BM) was conducted as previously described.[23] Briefly, AGE-modified substrate (AGE-BM) was produced by preincubating the BM matrix in a solution of 0.1 to 100 mM glycolaldehyde (for 4 hours at 37°C). To ensure no contamination with free glycating agents, the substrate was washed carefully five times with PBS. Any free aldehyde groups remaining were neutralized by incubating with 50 mM sodium borohydride (Sigma-Aldrich) overnight at 4°C. The substrate was further washed as just described before seeding with cells. In addition control matrices (unmodified BM) were produced in exactly the same way except for the step in which the glycolaldehyde glycating agent is added. The AGE-BM was washed thoroughly with PBS five times before all experiments. The degree of AGE modification and collagen cross-linking in this model substrate has been described by Stitt et al.[23]

Ultrastructural Evaluation of Cells on AGE-BM

ARPE-19 cells growing for 1 month on BM or AGE-BM were processed for transmission electron microscopy (TEM) by overnight fixation (in situ) in 2.5% glutaraldehyde in 0.1 M sodium cacodylate buffer (pH 7.2) for 30 minutes at room temperature. They were then postfixed in 1% osmium tetroxide, washed several times in 0.1 M cacodylate buffer and dehydrated in an ascending series of alcohol. The cells and their plastic dishes were then embedded in Spurr's resin. Sections were then cut and stained with uranyl acetate and lead citrate and viewed in a transmission electron microscope (H-7000; Hitachi Scientific Instruments, Finchhampstead, UK).

DNA Microarray Analysis

Hybridization. Total RNA was extracted from ARPE-19 exposed to unmodified (control) BM and AGE-BM for 1 month (Tri Reagent; Sigma-Aldrich), according to the manufacturer's instructions, and purified (RNeasy Mini Kit; Qiagen, Crawley, UK) with residual DNA removed by DNase I digestion (Qiagen). The quantity of RNA in each sample was determined spectrophotometrically (NanoDrop Technologies, LabTech International, Lewes, UK) and the integrity confirmed by 1% agarose gel electrophoresis.

Human 1 cDNA microarrays containing ~12,000 amplified cDNA clones from sequence-verified clone sets (Incyte; Open Biosystems, Huntsville, AL) were purchased from Agilent Technologies (Cheshire, UK), and cDNA targets were indirectly labeled (Genisphere 3DNA Submicro Expression Array detection kit; Genisphere Inc., Hatfield, PA). Briefly, total RNA was reverse transcribed using reverse transcription (RT) primers tagged with either an Alexa Fluor 546– or Alexa Fluor 647 (Invitrogen-Molecular Probes)–specific 3DNA capture sequence. The cDNAs were concentrated with a centrifugal filter (Microcon YM-30; Millipore Ltd., Watford, UK) and combined into one tube, and hybridization was performed according to the manufacturers' protocols. The tagged cDNAs were then fluorescently labeled by Alexa Fluor 546 or 647 via the complementary capture sequences.

Microarray Analysis. The microarray slides were scanned using a confocal laser scanner (ScanArray Lite; GSI Lumonics, Poole, UK) and images processed (ScanAlyze software; http://rana.lbl.gov/EisenSoftware.htm/ written by Michael Eisen and provided in the public domain by Eisen Lab, University of California, Berkeley, CA). Background-corrected intensities were calculated for each channel. *MvA* plots were generated (where M is the log intensity ratio and A is the log mean intensity), and Lowess normalization was performed.

A threshold of twofold change in expression was chosen to focus on an apt number of genes. To validate that changes of this magnitude were reliably detected, several genes (out of ~50) were chosen for further analysis by qRT-PCR. Seven genes agreed, and therefore it was reasonable to propose that most of the genes with greater than twofold difference were correctly assigned.

Validation by qRT-PCR. The results of the microarray were verified using qRT-PCR analysis of selected genes, on the same RNA sample used in the array and a second independent sample. qRT-PCR was performed on seven differentially expressed genes using a rapid thermal cycler system (LightCycler; Roche Molecular Biochemicals, UK), to monitor SYBR Green I fluorescence according to previously outlined protocols.[24] The specificity of the amplification reactions was

TABLE 1. Full Listings of Primer Sequences (5′–3′) for qRT-PCR Analysis

Gene Name	Accession Number	Forward Primer	Reverse Primer	Product (bp)
Thymosin	S54005	CTTCCCGCTCTCCACAGCCA	CGGGGGTAGGAAATCCTC	77
DAD1	U84214	GGACCTTCCCCTTCAACT	GGATGAAACTCCCCACAC	60
Adrenomodullin	NM_001124	GTGGGAAGAGGGAACTGCGG	CCTGTCTTCGGGGCTTCGAG	128
ApolipoproteinB	X04506	AAGTCCCGGAAGCCAGAGCC	GGGCACCCATCAGAAGCAGC	105
Metallothionein	X97261	TGTGCCGGCTCCTGCAAA	CACTTGGCACAGCCCACAGG	138
NET1	AK024919	TTGGTTCTGACTCGGCCCG	TCCTCGAAAGGAGCCTCCCA	135

confirmed by melting-curve analysis and relative expression levels quantified by reference to a standard dilution series.[25] For each gene, PCR amplifications were performed in triplicate on at least two independent RT reactions and normalized to GAPDH and 28S mRNA expression (primer pairs are listed in Table 1).

Lysosomal Enzyme Activity Assay

ARPE-19 cells were cultured on AGE-BM (0, 10, 50, and 100 mM GA modification) as described earlier and in parallel AGE-BM exposed ARPE-19 monolayers cultured from 0 to 28 days. Lysates were prepared for measurement of cathepsin-D enzymatic activity, as previously described,[26] ARPE-19 lysates were washed with PBS and incubated with Triton X-100 and 50 mM phosphate buffer, followed by 2% hemoglobin in 0.25 M sodium formate-buffered solution (pH 3.3) for 1 hour at 37°C. The reactions were stopped by incubation with ice cold 3% TCA. The samples were then centrifuged at 100 rpm for 5 minutes, and soluble proteolytic products measured using the BCA assay (Pierce Biotechnology, Rockford, IL) at A_{562} nm with tyrosine as a standard. The data were then converted to absolute tyrosine equivalents.

Autofluorescent Inclusions in ARPE-19 Monolayers

Photoreceptor outer segments (POS) were isolated as previously described[27] and stored at −20°C until use. ARPE-19 monolayers were cultured for 1 month on AGE-BM and control matrices, fed with POS (concentrations of 1×10^7/mL) every 48 hours between days 1 and 28 before being harvested by scraping into PBS and pelleted by centrifugation. At each appropriate time point, culture medium was removed by aspiration followed by the addition of trypsin-EDTA (200 μL) to detach cells. Cells were spun (250g, 4 mins, 4°C) to remove residual trypsin-EDTA and the pellet resuspended in 500 μL of PBS. Flow cytometry to identify inherent autofluorescence was performed according to previously reported methods.[28]

Statistical Analysis

Statistical analysis of the data obtained was performed by using commercial software to calculate the mean and SD (Excel; Microsoft, Redmond, WA). Subsequently, a one-way analysis of variance (ANOVA) with Bonferroni post hoc analysis, was conducted using another commercial package (SPSS, Chicago, IL). Data were considered significant at 95% ($P < 0.05$), where indicated.

RESULTS

AGEs in Clinical Samples

Spectral imaging of human Bruch's membrane showed the presence of autofluorescence with excitation emission spectra at 400- to 460-nm (the range associated with autofluorescent AGEs; Figs. 1B, 1D). Distinct from that observed with AGEs, autofluorescence of lipofuscin was also observed at a characteristic wavelength within the RPE cytoplasm (Figs. 1C, 1D).

Immunohistochemical analysis of GA-derived AGEs in the RPE and underlying Bruch's membrane choroid demonstrated

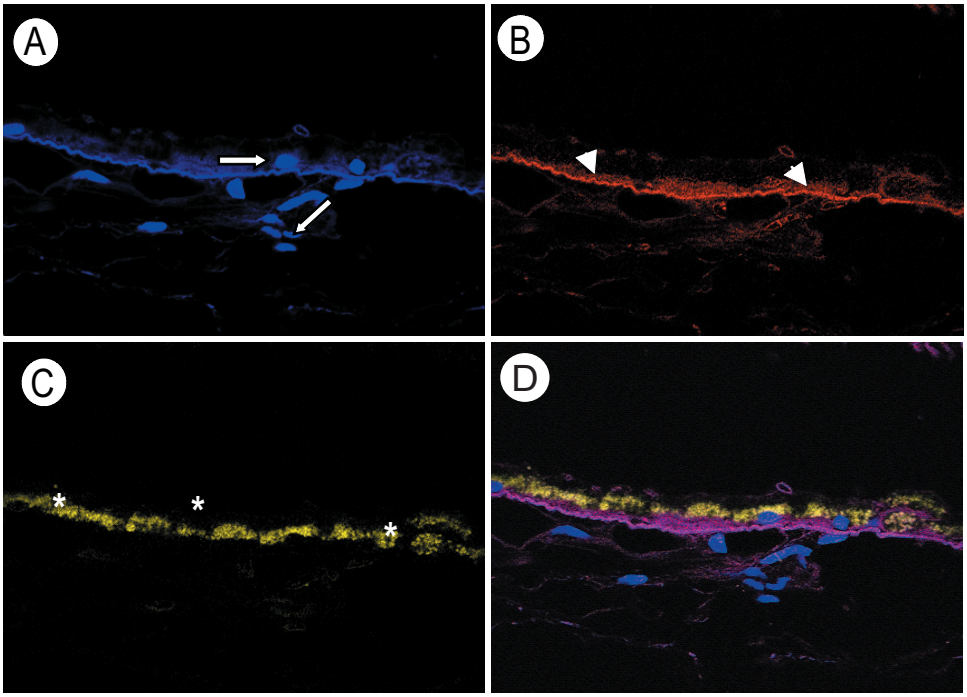

FIGURE 1. AGE-linked autofluorescence in human Bruch's membrane choroid. A spectral imaging system was used to determine the presence of AGE-linked autofluorescence in human specimens. Sections were assessed by confocal microscopy, using a λ scan approach to identifying areas of autofluorescence within each set wavelength. Each different band was then pseudocolored for ease of identification, as shown in a representative sample from an 88-year-old man with some evidence of drusen. (**A**) Cell nuclei stained with DAPI (*blue*, *arrows*). (**B**) Localization of fluorescent AGEs within the RPE layer and Bruch's membrane with excitation emission spectra in a 400- to 460-nm range (*red*; *left arrowhead*: AGEs at the level of Bruch's membrane; *right arrowhead*: AGEs in the RPE). The additional staining throughout the section is indicative of additional AGE accumulation in the collagenous choroid. (**C**) RPE autofluorescence (*yellow*) due to presence of lipofuscin (✶). (**D**) Composite image of (**A**–**C**). Original magnification, ×600.

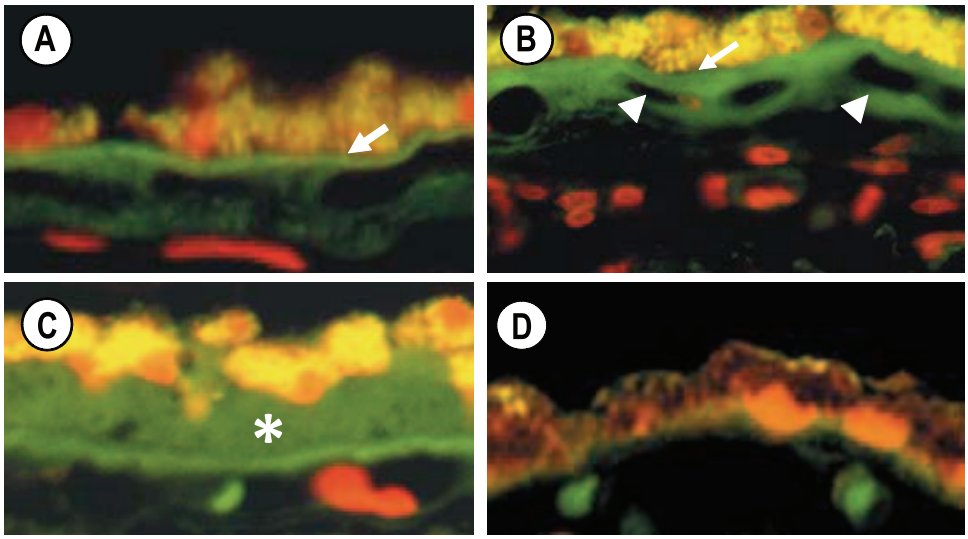

FIGURE 2. GA-derived AGE-immunoreactivity in human Bruch's membrane and choroid. Paraffin-embedded sections (7 μm) were subjected to immunolocalization by using specific monoclonal antibodies raised against GA-modified protein. (**A**) GA-derived immunoreactive adducts were evident in Bruch's membrane (*arrow*) in a 53-year-old donor. (**B**) Intense immunofluorescence for GA-adducts was also detected in a 76-year-old donor in Bruch's membrane (*arrow*), with more diffuse GA-immunoreactivity in the matrix around the choriocapillaris (*arrowheads*). (**C**) Immunoreactivity of these AGEs occurred in sub-RPE deposits (✶). (**D**) Typical autofluorescence of lipofuscin in the RPE was evident in all specimens and isotype-negative controls showed this characteristic autofluorescence of the RPE and to a degree, from the innermost collagenous layer of Bruch's membrane. In all images, nuclei are stained using PI. Original magnification, ×400.

the presence of significant AGE immunoreactivity at the level of Bruch's membrane (Fig. 2A). The intensity and extent of tissue immunoreactivity for GA-derived AGEs were elevated in elderly donors (>75 years), when compared to younger donors, thus reinforcing the suitability of GA for use in an in vitro model of Bruch's membrane ageing (compare Figs. 2A, 2B).

AGEs in ARPE-19 Monolayers

Phase-contrast microscopy demonstrated little difference in appearance between cells growing on a control unmodified BM or AGE-BM (Figs. 3A, 3B). However, TEM revealed marked ultrastructural abnormalities on AGE-exposed cells. Control ARPE-19 showed typical culture characteristics with tight junction formation, fully-formed smooth and rough endoplasmic reticulum (SER; RER), polyribosomes, numerous mitochondria, and lysosomal-like inclusions. By contrast, cells on an AGE-BM showed less evidence of tight junctions and many cells contained large, electron-lucent, lipidlike inclusions toward the basal side of the cytoplasm (compare Figs. 3C, 3D).

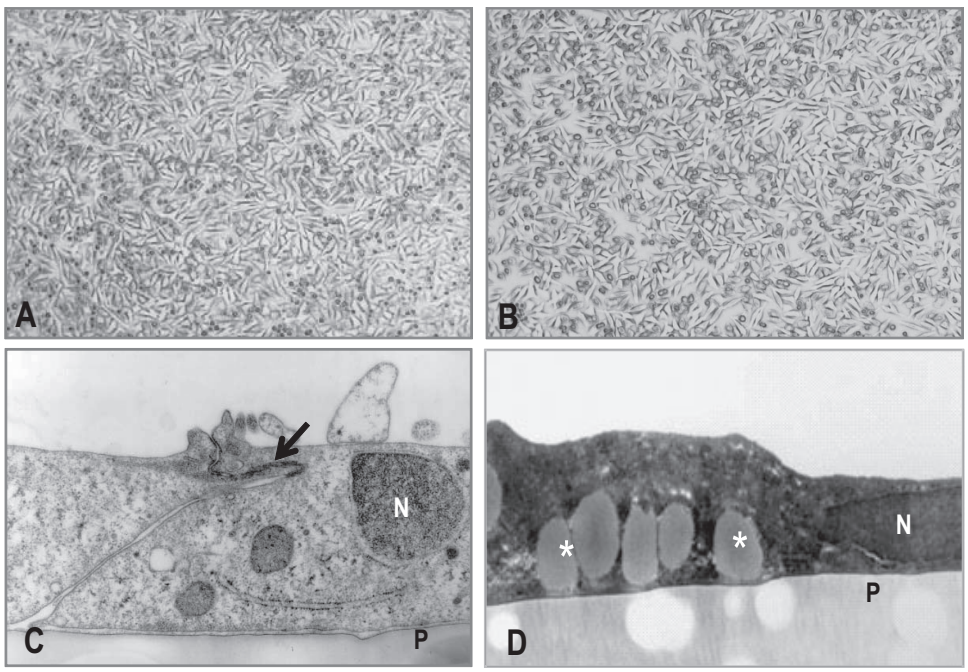

FIGURE 3. Morphologic changes associated with exposure to AGE-BM. Phase-contrast micrographs of ARPE-19 that were seeded onto control unmodified BM (**A**) and AGE-BM (**B**). On a gross level, the cells appeared similar across treatments. By contrast, ultrastructural evaluation of control (**C**) and AGE-exposed cells (**D**) revealed that large lipid-like inclusions (✶) occurred in cells growing on AGE-BM. These were located on the basal side of the cytoplasm. P, plastic of the culture dish; N, nucleus; *arrow*, tight junction. Magnification: (**A**, **B**) ×200; (**C**, **D**) ×20,000.

TABLE 2. RPE mRNAs Upregulated in Response to AGE-BM Exposure

Unigene Number	Chromosome Location	Gene	Function	Increase (*x*-fold)
Hs.490330	Chromosome 1	Natriuretic peptide receptor A/guanylate cyclase A [*NPR1*]	Gives guanylate cyclase activity.	8.6
Hs.500972	Chromosome 1	Ste20 related serine/threonine kinase [*SLK*]	Binds ATP and DNA, has nuclease activity	5.9
Hs.407190	Chromosome 6	FK 506-binding protein 5 [*FKBP5*]	Interacts with HSP90 and TEBP.	5.2
Hs.368157	Chromosome 20	Phosphorylase, glycogen, brain [*PYGB*]	Allosteric enzyme in carbohydrate metabolism.	3.3
Hs.50861	Chromosome 12	Sir-2 like 4 [*SIRT4*]	Probable NAD dependent deacetylase.	3.3
Hs.432818	Chromosome 5	Microfibrillar-associated protein 3 [*MFAP3*]	Component of elastin-associated microfibrils.	3.3
Hs.109514	Chromosome 1	Ryanodine receptor 2 (cardiac) [*RYR2*]	Involved in communication between transverse tubules and the sarcoplasmic reticulum.	3.2
Hs.12967	Chromosome 6	Synaptic nuclei expressed gene 1b [*SYNE1*]	Involved in maintenance of nuclear organization and structural integrity.	3.0
Hs.479944	Chromosome 12	Peroxisome receptor 1 [*PEX5*]	Binds to C-terminal PTS1-type tripeptide peroxisomal targeting signal (SKL-type), has role in peroxisomal protein import.	3.0
Hs.502836	Chromosome 11	ADP-ribosylation factor-like 2 [*ARL2*]	Component of regulated secretory pathway involved in Ca (2+)-dependent release of acetylcholine.	2.9
Hs.515560	Chromosome 19	Kallikrein-related peptidase 2 [*KLK2*]	Cleaves Met-Lys and Arg-Ser bonds in kininogen and enables release of Lys-bradykinin.	2.9
Hs.458273		Metallothionein IL [*MTIL*]	Binds heavy metals. Transcriptionally regulated by heavy metals and glucocorticoids.	2.8
Hs.11776	Chromosome 1	U4/U6-associated RNA splicing factor [*PRPF3*]	Participant in pre-mRNA splicing. May play a role in assembly of U4/U5/U6 tri-snRNP complex.	2.6
Hs.29499	Chromosome 4	Toll like receptor 3 [*TLR3*]	Participant in innate immune response. May have role in recognition of ds-RNA. Action via MyD88 and TRAF6, leading to NFκB activation.	2.5
Hs.368160	Chromosome 5	Protocadherin 43/Protocadherin gamma subfamily C, 3 [*PCDHGC3*]	Calcium-dependent cell adhesion protein. Involved in establishment and maintenance of neuronal connections.	2.3
Hs.435556	Chromosome 16	Apoptosis regulator [*BFAR*]	Promoter of cell survival. Supressor of BAX-induced apoptosis.	2.1
Hs.441047	Chromosome 11	Adrenomedullin [*ADM*]	Hypotensive and vasodilatatory agent. Control of homeostasis, hypotensive effects in vessels.	2.1
Hs.515126	Chromosome 19	Intracellular adhesion molecule 1 (ICAM1/CD 54) [*ICAM1*]	Ligand for leukocyte adhesion LFA-1 protein (Integrin alpha-L/beta-2).	2.1
Hs.434971	Chromosome X	Trophinin [*TRO*]	Directly responsible for homophilic cell adhesion. Potential involvement with tastin and bystin in cell adhesion molecule complex.	2.0
Hs.446574	Chromosome 2	Thymosin, beta 10 [*TMSB10*]	Cytoskeletal organization. Binds and sequesters G actin monomers, inhibits actin polymerization.	2.0

mRNA/Microarray Analysis

Exposure of ARPE-19 monolayers to AGE-BM induced both up- and downregulation of a wide range of mRNAs when compared to cells grown on a native (control) substrate (Tables 2, 3). Microarray analysis was performed on a single sample set; therefore, parallel qRT-PCR was necessary to confirm array results. qRT-PCR was performed on both the sample used for the microarray and on an additional biological replicate to validate the dataset. Microarray spots with greater than twofold change were chosen for additional analysis, and seven mRNAs were selected (Figs. 4, 5). Those with altered gene expression could be further analyzed and categorized into functional groupings such as the metalloproteinases, cathepsins, lysosomal/degradative enzymes, and genes associated with attachment, spreading, and immune responses using the DAVID bioinformatics database (http://david.abcc.ncifcrf.gov/ provided in the public domain by the National Institute for Allergy and Infectious Diseases, Bethesda, MD). All genes tested were confirmed by predictive analysis. Array data are tabulated in Tables 2 and 3.

qRT-PCR was conducted on a range of mRNA candidates from the array data that showed up- or downregulation on exposure to AGE-BM. Using these selected mRNAs, the changes revealed by the array data were confirmed by qRT-PCR analysis. In all the examples chosen, comparable and significant ($P < 0.05$) changes were observed in comparison between ARPE-19 cells grown on BM and those grown on AGE-BM (Figs. 4, 5).

Lysosomal Enzyme Activity

Microarray analysis revealed a significant downregulation of a range of mRNAs encoding for lysosomal and degradative enzymes such as the cathepsins on ARPE-19 exposed to AGE-BM (Tables 2, 3). This finding led to a more thorough investigation of lysosomal enzyme mRNAs using qRT-PCR. Cathepsin-D is a key RPE lysosomal enzyme with reported

TABLE 3. RPE mRNAs Downregulated in Response to AGE-BM Exposure

Unigene Number	Chromosome Location	Gene	Function	Decrease (*x*-fold)
Hs.518270	Chromosome 3	Solute carrier family 21 (prostaglandin transporter), member 2 [*SLCO2A1*]	Transports PGD2, PGE1, PGF2 and PGF2A. May mediate release and transepithelial transport of newly synthesized prostaglandins.	17.2
Hs.436893	Chromosome 13	Solute carrier family 15 (oligopeptide transporter), member 1 [*SLC15A1*]	Proton-coupled intake of oligopeptides (2-4 amino acids), with dipeptide preference.	9.1
Hs.120759	Chromosome 2	Apolipoprotein B (including Ag [x] antigen) [*APOB*]	Recognition signal for cellular binding and internalization of LDL particles by apoB/E receptor.	5.0
Hs.1290	Chromosome 5	Complement component C9 [*C9*]	Final component added in MAC formation. Responsible for formation of transmembrane channels.	5.0
Hs.80485	Chromosome 3	Adipose most abundant gene transcript 1 [*ACDC*]	Negative regulator in haematopoesis. Inhibits endothelial NFκB signalling via cAMP dependent pathway. Inhibits TNFα expression of endothelial adhesion molecules.	4.2
Hs.1408	Chromosome 20	Endothelin 1 [*EDN3*]	Endothelium derived vasoconstrictor.	4.0
Hs.415768	Chromosome 17	Nerve growth factor receptor (TNFR superfamily, member 16). [*NGFR*]	Low-affinity receptor for NGF, BDNF, NT-3/NT-4 and mediates survival and cell death of neural cells.	3.9
Hs.524368	Chromosome 12	Vitamin D (1, 25-dihydroxyvitamin D3) receptor. [*VDR*]	Nuclear hormone receptor. Mediator of vitamin D3 action.	3.8
Hs.317632	Chromosome 5	Cadherin 18, type 2 [*CDH1*]	Calcium dependent cell adhesion protein.	3.7
Hs.591484	Chromosome 1	Laminin gamma 2 [*LAMC2*]	Mediator of attachment, migration and organization of cells to tissues in embryogenesis by extracellular matrix interactions. Ladsin exerts cells scattering activity.	3.5
Hs.632402	Chromosome 1	Connexin 59 gene [*CX59/GJA10*] or gap junction protein, alpha 10, 59kDa	Involved in the action of connexons, through which low-MW materials diffuse through cells.	3.5
Hs.82890	Chromosome 14	Defender against cell death 1 [*DAD1*]	DAD1 loss triggers apoptosis.	3.4
Hs.138378	Chromosome 11	Caspase 4-apoptosis related cysteine protease [*CASP4*]	Role in activation cascade of caspases, responsible for the execution of apoptosis.	3.2
Hs.5302	Chromosome 19	Lectin, galactoside binding soluble (galectin 4) [*LGALS4*]	Binds lactose and related sugars. May be involved in the assembly of adherens junctions.	3.1
Hs.35354	Chromosome 3	IGF-II mRNA binding protein 2 [IMP-2]	Nuclear mRNA splicing.	3.0
Hs.2258	Chromosome 11	Matrix metalloproteinase 10 (stromelysin 2) [*MMP10*]	Degrades fibronectin, type I, III, IV and V gelatins and collagen III, IV and V. Activates procollagenase.	3.0
Hs.25155	Chromosome 10	Neuroepithelial cell transforming gene 1 [*NET1*]	Acts as guanine nucleotide exchange factor (GEF) for RhoA GTPase. May activate SAPK/JNK pathway.	2.9
Hs.421724	Chromosome 14	Cathepsin G [*CTSG*]	Proteolysis and peptidolysis.	2.9
Hs.443031	Chromosome 3	Lysosomal beta galactosidase [*GLB1*]	Essential for activity of β galactosidase and neuraminidase. Can deamidate tachykinins.	2.8

alterations during aging,[29] and so this candidate was chosen for qRT-PCR analysis. When exposed to AGE-BM, ARPE-19 showed significant downregulation of cathepsin-D mRNA ($P < 0.05$; Fig. 6A). After the array and qRT-PCR analysis, cathepsin-D-linked proteolytic activity from 14 days was significantly reduced in ARPE-19 cultures exposed to modified AGE-BM ($P < 0.05$; Figs. 6B, 6C).

Lipofuscin Accumulation

Lipofuscin-associated autofluorescence at wavelengths associated with RPE lipofuscin was measured in ARPE-19 cells growing on native BM and AGE-BM and also on a separate group coexposed to POS (1×10^7 segments/mL). The AGE-modified substrate induced a moderate but significant increase in autofluorescence when compared to ARPE-19 grown on native BM ($P < 0.05$; Fig. 7). However, when cells were exposed to POS, the AGE-BM group demonstrated a marked increase in accumulation of autofluorescent lipofuscin-like material ($P < 0.01$; Fig. 7).

DISCUSSION

AGEs accumulate on long-lived skin and lens proteins in the elderly.[30] A progressive elevation of these pathogenic adducts also occurs on Bruch's membrane where they could make a significant contribution to age-related RPE dysfunction. AGE accumulation in Bruch's membrane-RPE has been reported by several groups,[11,12,14–16,31,32] but this is the first time that GA-derived AGEs have been shown in this tissue. AGE generation can occur via a variety of reactive α-oxaloaldehydes, and we have previously used GA as an in vitro AGE-forming substance and characterized the resultant AGE-adducts and degree of cross-linking.[23] GA-derived AGEs have been shown previously to induce RPE attachment abnormalities and cause reduced viability[33,34] and therefore, as

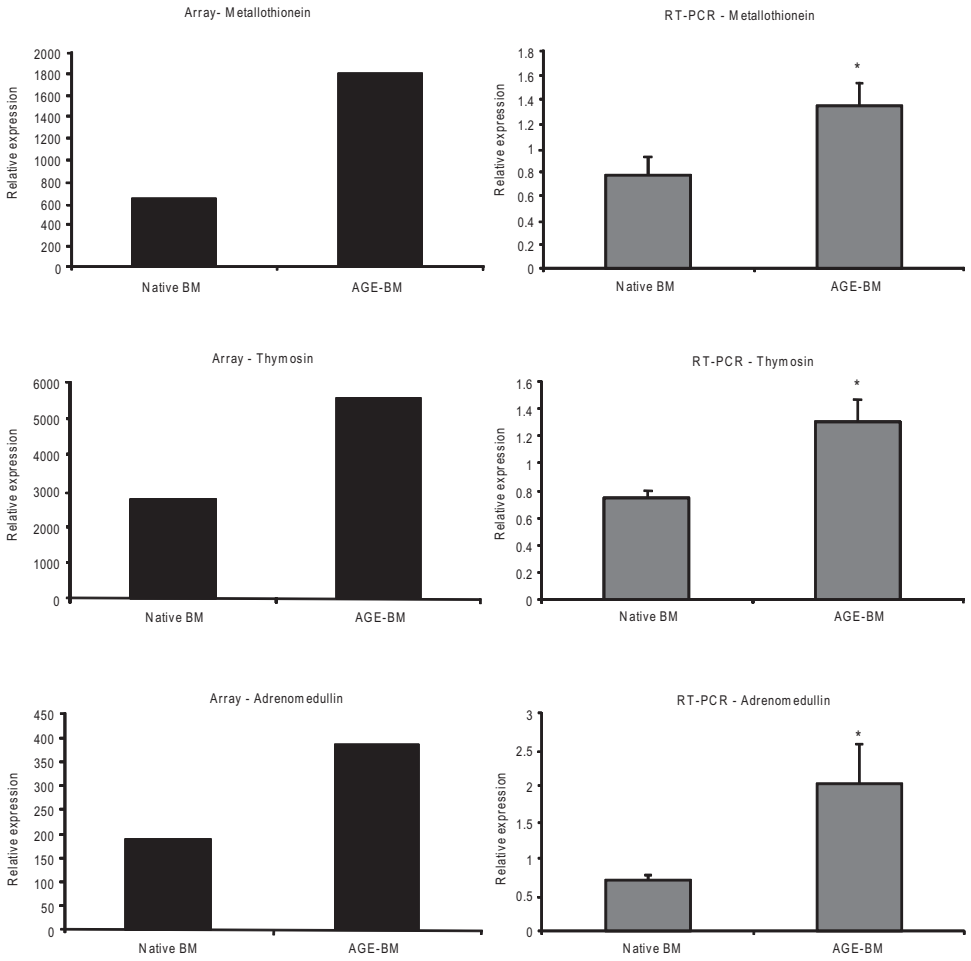

FIGURE 4. ARPE-19 mRNAs upregulated in response to AGE-BM: comparison of array and qRT-PCR. A selection of ARPE-19 mRNAs found to be altered by AGE-BM exposure using microarray analysis were subsequently analyzed using qRT-PCR. Metallothionein was upregulated in response to the AGE-BM, and this was confirmed by qRT-PCR. Upregulation of thymosin was demonstrated on the array after exposure to AGE-BM and was subsequently confirmed by qRT-PCR. Microarray analysis also revealed that adrenomedullin was upregulated in response to the AGE-BM (confirmed by qRT-PCR; $^*P < 0.05$).

an AGE-forming agent, this α-oxaloaldehyde is a physiologically relevant choice for subsequent in vitro studies.

It has been reported that differences exist in the genetic profiling of primary RPE versus ARPE-19 cells, although none of our significantly regulated genes fall into this category.[35] Therefore, the use of the ARPE-19 immortalized cell line is appropriate for this study, as it exhibits many characteristics of primary human RPE. Noticeable differences in ARPE-19 gene expression levels have also been reported with changes in environment and in age (passage number).[35–37] To this end, all cells in this study were cultured and used at a consistent passage and differentiation state.

The microarray investigation conducted in the present study has established a considerable dataset of both up- and downregulated ARPE-19 mRNAs in response to prolonged exposure to AGE-BM. A similar global analysis has been conducted on "aged" RPE cells from galactose-treated mice,[17] and that study identified significant alterations in mRNA expression of stress response elements and genes encoding extracellular matrix production/modification and proinflammatory responses. Other studies have identified significant gene clusters relating to ARPE-19 differentiation, cell cycle regulation, early apoptosis, and Bruch's membrane remodeling after short-term (4-hour) RPE exposure to oxidative insults.[38,39] Functional clustering analysis in our study using DAVID functional annotations highlighted enrichment for extracellular matrix genes ($P < 0.005/P = 0.0029$) and signal peptides ($P < 0.001/P =$ 0.00,091). Functional clustering with high stringency, established the importance of alterations to lysosomal enzyme gene expression levels (cathepsin-S, -D, and -G; β-galactosidase; lysosomal beta mannosidase; and acid phosphatase) and the expression of structurally important proteases such as several matrix metalloproteinases and collagenases support previously published results.[40,41]

The transcriptional response of several genes altered by oxidative stress and programmed cell death were also significantly altered in both our mRNA analyses. For example, a twofold upregulation of the mRNA encoding thymosin β10 was observed, and this gene product has links to wound repair and cytoskeletal organization via modulation of actin polymerization. It also plays a potential role in the attenuation of RPE damage after oxidative stress.[42] Of interest, metallothionein was also upregulated (2.8-fold) by ARPE-19 cells in response to oxidant stress.[43]

The most significantly upregulated mRNAs in response to AGE-BM exposure were guanylate cyclase A, and Ste-20 serine/threonine kinases. The natriuretic peptide system has a significant role in the retina and can modulate vascular permeability and angiogenesis.[44] Serine/threonine kinases play a role in ATP/DNA binding activity and are effected by the cytokine, transforming growth factor-β,[45] playing a role in cell differentiation, apoptosis, and proliferation (Table 2).

The most significantly downregulated mRNA was prostaglandin transporter SLC21a2 (Table 3). Information in relation to SLC21a2 in retinal disease is sparse, although prostaglandin levels are known to be altered by AGE exposure in mesothelial cells[46] and retinal pericytes.[47] The prostaglandin transporter is widely expressed in the retina[48] and is known to transport prostaglandin D-2 synthase to prevent reactive oxygen species

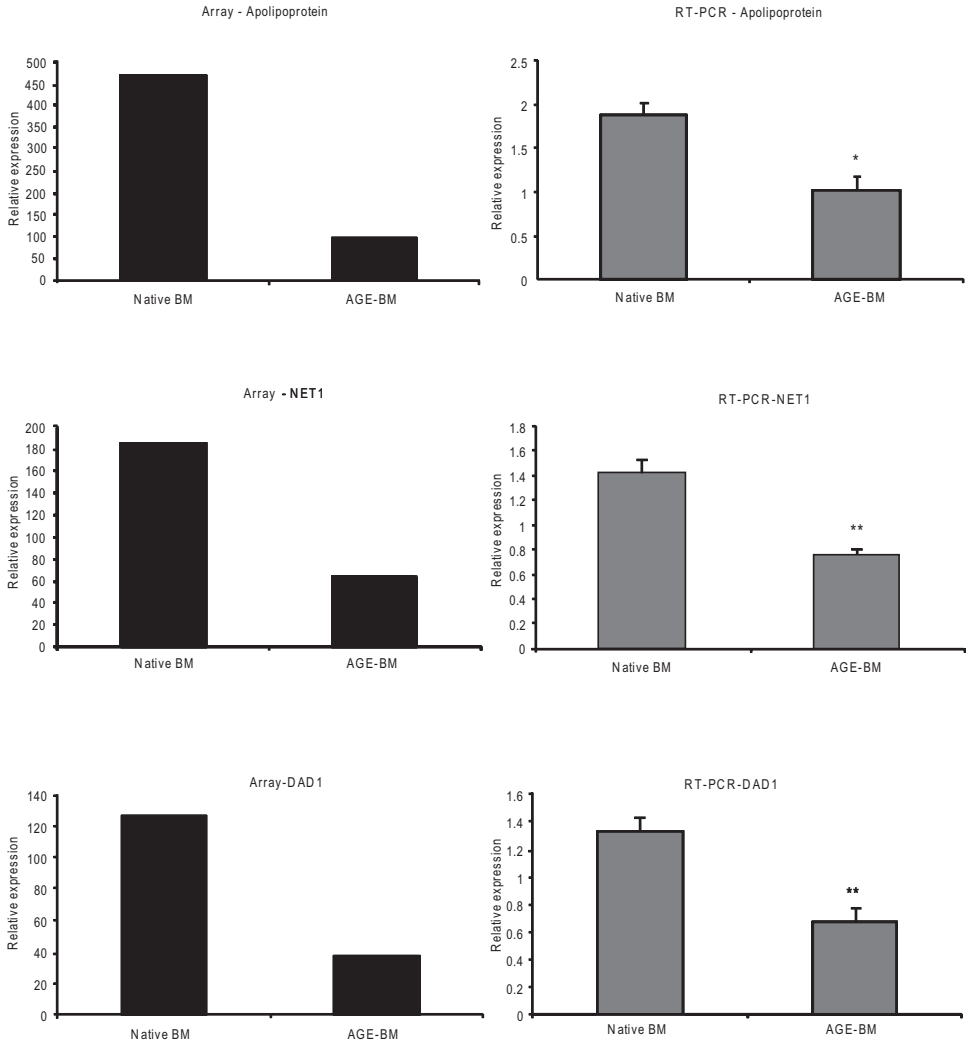

FIGURE 5. ARPE-19 mRNAs downregulated in response to AGE-BM: comparison of array and qRT-PCR. Apolipoprotein B was downregulated after exposure to the AGE-BM, and this result was subsequently confirmed by qRT-PCR. Analysis of the microarray also revealed that NET1 was downregulated in response to the AGE-BM, which was further confirmed by qRT-PCR. DAD1 was also found to be downregulated in response to the AGE-BM, and qRT-PCR also confirmed this result ($^{**}P \leq 0.001$, $^{*}P < 0.05$).

(ROS) generation.[49] This may link to the potential for AGEs to induce oxidative stress in various cell types.[50–53]

The mechanism through which exposure to AGE-BM alters RPE gene expression is relatively unknown. Previous work in our laboratory has identified an upregulation of components of the AGE receptor complex—in particular galectin-3 (AGER3), found on RPE (D407) exposure to AGE-modified albumin.[20] It is likely that prolonged exposure of RPE to AGE-BM, as occurs in normal aging, stimulates a progressive oxidative insult. It should be borne in mind that this study is based on the ARPE-19 human cell line that exhibits a lack of melanosomes, which may alter the antioxidant capacity because these organelles bind divalent cations that could be used in the Fenton reaction. However, the antioxidant potential of the RPE remains equivocal, and a recent report suggests that melanosomes have little antioxidant activity.[54] Indeed, in aged individuals, the melanosomes actually become toxic.[55–57] Thus, if anything, the presence of melanosomes would most likely potentiate the effect of AGE-BM.

Increased oxidative stress can occur as a direct result of AGE receptor signaling,[12] which, in itself, can lead to direct upregulation of antioxidant defenses.[58] In particular RAGE has been identified in subretinal membranes of patients with AMD[59] and in macular RPE overlying basal laminar deposits[21] and photoreceptors from AMD donors where it colocalizes with immunoreactive AGEs.[12] RAGE-receptor activation, if it occurs, could transduce several cellular responses, including the activation of antioxidant defenses via initiation of NFκB transcription.[54] It is possible that AGE-BM, through interaction with one or more AGE receptors, could lead to a prolonged oxidative insult, thus evoking RPE defense mechanisms. Recent studies have also linked the pathogenic significance of RAGE activation through direct induction of VEGF secretion within ARPE-19 cultures.[21]

The mRNAs encoding the cysteine thiol proteases cathepsin-S and -G and the lysosomal enzymes acid phosphatase, β-galactosidase, and β-mannosidase were significantly downregulated in AGE-BM-exposed ARPE-19 monolayers. This is an important finding, because it is now widely recognized that lysosomal enzymes are susceptible to age-related changes.[60] Previous studies have demonstrated an age-related decrease in the activity of several RPE glycosidases, including β-galactosidase.[61] Hjelmeland et al.[62] have shown that senescent RPE cultures accumulate β-galactosidase-positive cells as a function of population-doubling time. Recent studies have also identified the alteration of several cathepsins under conditions of high oxidative burden.[53] The significant role of initiators of oxidative stresses (e.g., ROS, free radicals, and AGEs) and the resultant lysosomal dysfunction are clearly evident from all data sets under investigation in this study.

Lysosomal dysfunction is of prime importance in RPE age-related disease, and lipofuscin accumulates in these cells as a direct result of impaired degradative pathways.[63] It has been demonstrated that there is a downregulation of lysosomal as-

partic and cysteine cathepsin mRNA expression and enzymatic activity in the glomeruli of diabetic rats[64] and in tubule epithelium in response to AGE exposure.[65] The current array data have included assessment of AGE-BM-associated changes in lysosomal enzyme mRNA expression, and significant alterations have been confirmed by qRT-PCR analysis. Such findings have been further strengthened by the observed reduction of cathepsin-D enzymatic activity in AGE-BM exposed ARPE-19

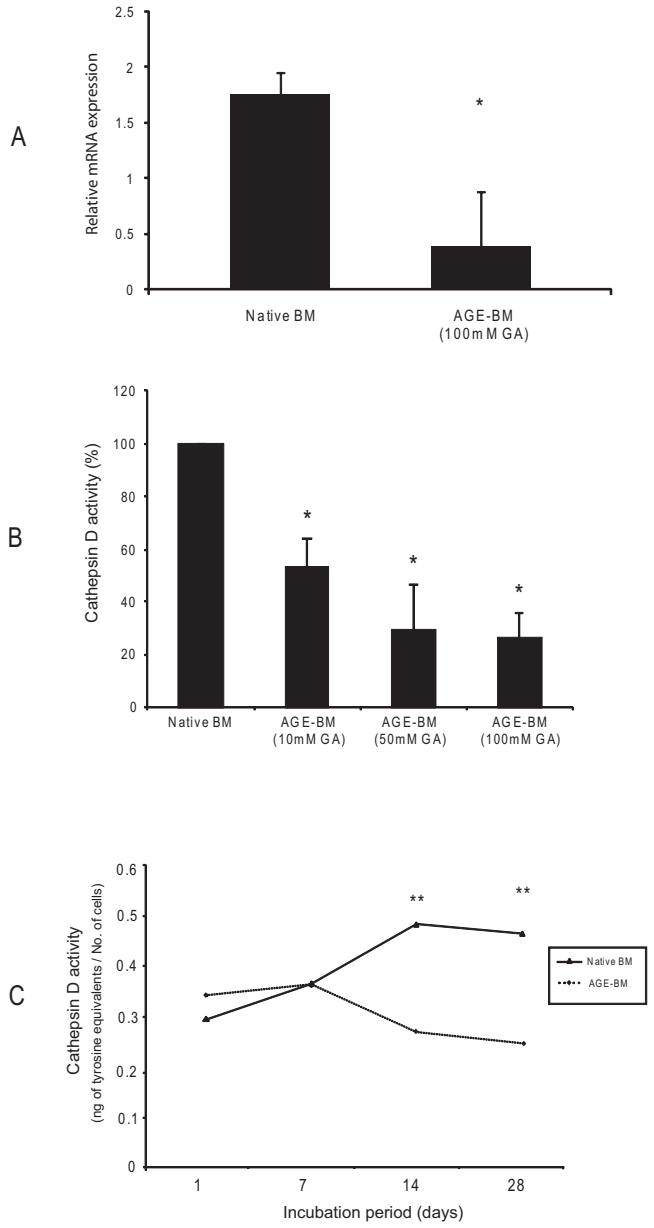

FIGURE 6. ARPE-19 grown on AGE-BM shows attenuated cathepsin-D expression and activity. (**A**) ARPE-19 cell monolayers were cultured on native BM or AGE-BM for 28 days, and cathepsin-D mRNA was analyzed by qRT-PCR. AGE exposure resulted in a significant reduction in cathepsin-D expression ($n = 3$; $^{*}P < 0.05$). (**B**) Cathepsin-D enzymatic activity was also significantly decreased in accordance with increasing AGE modification of the BM (10–100 mM GA) when compared to native BM controls ($n = 3$; $^{*}P < 0.0.5$). (**C**) Cathepsin-D activity was monitored over a time course for up to 28 days on native BM or AGE-BM (100 mM GA). Activity was significantly suppressed after 14 days of treatment ($n = 3$, $^{**}P < 0.01$). All values were normalized to a medium only control. *y*-Axis label indicates nanograms of tyrosine equivalents per 10^3 cells.

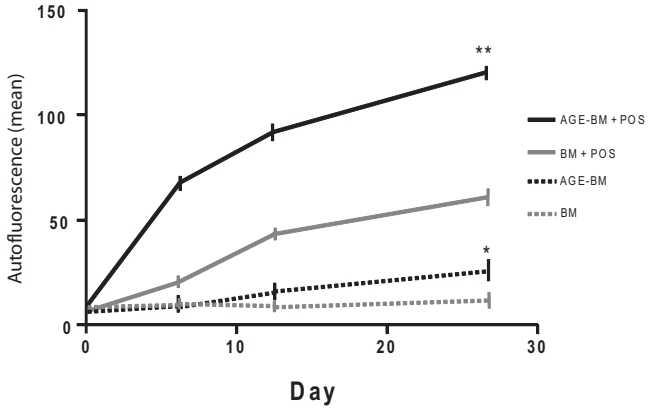

FIGURE 7. Exposure to AGE-BM increases lipofuscin in ARPE-19 monolayers. Low levels of fluorescence were detectable over the full 28 days in medium-only control cells (BM), with marginal increases detectable in cells grown on a glycated matrix (AGE-BM) only, indicating incorporation into the cell lysosome of glycated matrix components. Significant autofluorescent increases were noted when cells were exposed to both POS and AGE-BM matrices with the most significant increases ($^{*}P < 0.05$) occurring after 14 days of exposure, with maximum increases at 28 days ($^{**}P < 0.01$) datasets that parallel the microarray analyses time course.

and are likely to be linked to the observed accumulations of lipofuscin in these cells. It has also been recently reported that peroxidation and reactive aldehyde activity can increase the resistance of POS to cleavage and proteolysis by lysosomal cathepsins.[66] The present study has shown that AGE-BM results in a decrease in cathepsin-D enzymatic activity. Dysfunction of this enzyme has been associated with increased accumulation of autofluorescent inclusions in the RPE both in vitro and in vivo and enhanced accumulation of autofluorescent material occurs on AGE-BM membranes.[27–29,67,68] Therefore, it is not unreasonable to conclude that accumulation of autofluorescent material on AGE-BM membranes is due to a decrease in lysosomal enzyme activity.

Taken together, AGEs appear to play an important role in age-related dysfunction of the RPE. The use of complementary proteomic technologies is ongoing in our laboratory and should provide further insight into how Bruch's membrane-immobilized AGEs modulate pathophysiological responses in ARPE-19 monolayers. Indeed, further investigation is warranted to dissect the effects that AGE adduct formation has on RPE function. Such studies would also serve to highlight the potential for agents that can prevent or even break established AGE-protein cross-links in the context of retinal ageing.

Acknowledgments

The authors thank the Bristol Eye Bank for provision of donor tissues.

References

1. Zarbin MA. Current concepts in the pathogenesis of age-related macular degeneration. *Arch Ophthalmol.* 2004;122:598–614.
2. Okubo A, Rosa RH Jr, Bunce CV, et al. The relationships of age changes in retinal pigment epithelium and Bruch's membrane. *Invest Ophthalmol Vis Sci.* 1999;40:443–449.
3. Karwatowski WS, Jeffries TE, Duance VC, Albon J, Bailey AJ, Easty DL. Collagen and ageing in Bruch's membrane. *Biochem Soc Trans.* 1991;19:349S.
4. Karwatowski WS, Jeffries TE, Duance VC, Albon J, Bailey AJ, Easty DL. Preparation of Bruch's membrane and analysis of the age-related changes in the structural collagens. *Br J Ophthalmol.* 1995;79:944–952.

5. Pauleikhoff D, Harper CA, Marshall J, Bird AC. Aging changes in Bruch's membrane: a histochemical and morphologic study. *Ophthalmology.* 1990;97:171–178.
6. Sheraidah G, Steinmetz R, Maguire J, Pauleikhoff D, Marshall J, Bird AC. Correlation between lipids extracted from Bruch's membrane and age. *Ophthalmology.* 1993;100:47–51.
7. Coffey AJ, Brownstein S. The prevalence of macular drusen in postmortem eyes. *Am J Ophthalmol.* 1986;102:164–171.
8. Baynes JW. The role of AGEs in aging: causation or correlation. *Exp Gerontol.* 2001;36:1527–1537.
9. Monnier VM, Sell DR, Nagaraj RH, et al. Maillard reaction-mediated molecular damage to extracellular matrix and other tissue proteins in diabetes, aging, and uremia. *Diabetes.* 1992;41(suppl 2):36–41.
10. Thornalley PJ. The enzymatic defence against glycation in health, disease and therapeutics: a symposium to examine the concept. *Biochem Soc Trans.* 2003;31:1341–1342.
11. Handa JT, Verzijl N, Matsunaga H, et al. Increase in the advanced glycation end product pentosidine in Bruch's membrane with age. *Invest Ophthalmol Vis Sci.* 1999;40:775–779.
12. Howes KA, Liu Y, Dunaief JL, et al. Receptor for advanced glycation end products and age-related macular degeneration. *Invest Ophthalmol Vis Sci.* 2004;45:3713–3720.
13. Glenn JV, Beattie JR, Barrett L, et al. Confocal Raman microscopy can quantify advanced glycation end product (AGE) modifications in Bruch's membrane leading to accurate, nondestructive prediction of ocular aging. *FASEB J.* 2007;21(13):3542–3552.
14. Ishibashi T, Murata T, Hangai M, et al. Advanced glycation end products in age-related macular degeneration. *Arch Ophthalmol.* 1998;116:1629–1632.
15. Schutt F, Bergmann M, Holz FG, Kopitz J. Proteins modified by malondialdehyde, 4-hydroxynonenal, or advanced glycation end products in lipofuscin of human retinal pigment epithelium. *Invest Ophthalmol Vis Sci.* 2003;44:3663–3668.
16. Yamada Y, Ishibashi K, Bhutto IA, Tian J, Lutty GA, Handa JT. The expression of advanced glycation endproduct receptors in RPE cells associated with basal deposits in human maculas. *Exp Eye Res.* 2006;82:840–848.
17. Tian J, Ishibashi K, Reiser K, et al. Advanced glycation endproduct-induced aging of the retinal pigment epithelium and choroid: a comprehensive transcriptional response. *Proc Natl Acad Sci U S A* 2005;102:11846–11851.
18. Ida H, Ishibashi K, Reiser K, Hjelmeland LM, Handa JT. Ultrastructural aging of the RPE-Bruch's membrane-choriocapillaris complex in the D-galactose-treated mouse. *Invest Ophthalmol Vis Sci.* 2004; 45:2348–2354.
19. Yasukawa T, Wiedemann P, Hoffmann S, et al. Glycoxidized particles mimic lipofuscin accumulation in aging eyes: a new age-related macular degeneration model in rabbits. *Graefes Arch Clin Exp Ophthalmol.* 2007;245:1475–1485.
20. McFarlane S, Glenn JV, Lichanska AM, Simpson DA, Stitt AW. Characterisation of the advanced glycation endproduct receptor complex in the retinal pigment epithelium. *Br J Ophthalmol.* 2005;89:107–112.
21. Ma W, Lee SE, Guo J, et al. RAGE Ligand Upregulation of VEGF Secretion in ARPE-19 Cells. *Invest Ophthalmol Vis Sci.* 2007;48: 1355–1361.
22. Dunn KC, Aotaki-Keen AE, Putkey FR, Hjelmeland LM. ARPE-19, a human retinal pigment epithelial cell line with differentiated properties. *Exp Eye Res.* 1996;62:155–169.
23. Stitt AW, Hughes SJ, Canning P, et al. Substrates modified by advanced glycation end-products cause dysfunction and death in retinal pericytes by reducing survival signals mediated by platelet-derived growth factor. *Diabetologia.* 2004;47:1735–1746.
24. Feeney SA, Simpson DA, Gardiner TA, Boyle C, Jamison P, Stitt AW. Role of vascular endothelial growth factor and placental growth factors during retinal vascular development and hyaloid regression. *Invest Ophthalmol Vis Sci.* 2003;44:839–847.
25. Simpson DA, Feeney S, Boyle C, Stitt AW. Retinal VEGF mRNA measured by SYBR green I fluorescence: A versatile approach to quantitative PCR. *Mol Vis.* 2000;6:178–183.
26. Schutt F, Davies S, Kopitz J, Holz FG, Boulton ME. Photodamage to human RPE cells by A2-E, a retinoid component of lipofuscin. *Invest Ophthalmol Vis Sci.* 2000;41:2303–2308.
27. Wassell J, Ellis S, Burke J, Boulton M. Fluorescence properties of autofluorescent granules generated by cultured human RPE cells. *Invest Ophthalmol Vis Sci.* 1998;39:1487–1492.
28. Rakoczy P, Kennedy C, Thompson-Wallis D, Mann K, Constable I. Changes in retinal pigment epithelial cell autofluorescence and protein expression associated with phagocytosis of rod outer segments in vitro. *Biol Cell.* 1992;76:49–54.
29. Rakoczy PE, Lai CM, Baines M, Di Grandi S, Fitton JH, Constable IJ. Modulation of cathepsin D activity in retinal pigment epithelial cells. *Biochem J.* 1997;324:935–940.
30. Sell DR, Monnier VM. Conversion of arginine into ornithine by advanced glycation in senescent human collagen and lens crystallins. *J Biol Chem.* 2004;279:54173–54184.
31. Radeke MJ, Peterson KE, Johnson LV, Anderson DH. Disease susceptibility of the human macula: differential gene transcription in the retinal pigmented epithelium/choroid. *Exp Eye Res.* 2007;85: 366–380.
32. van Soest SS, de Wit GM, Essing AH, et al. Comparison of human retinal pigment epithelium gene expression in macula and periphery highlights potential topographic differences in Bruch's membrane. *Mol Vis.* 2007;13:1608–1617.
33. Wang Z, Paik DC, Del Priore LV, Burch RL, Gaillard ER. Nitrite-modified extracellular matrix proteins deleteriously affect retinal pigment epithelial cell function and viability: a comparison study with nonenzymatic glycation mechanisms. *Curr Eye Res.* 2005;30: 691–702.
34. Verzijl N, DeGroot J, Thorpe SR, et al. Effect of collagen turnover on the accumulation of advanced glycation end products. *J Biol Chem.* 2000;275:39027–39031.
35. Cai H, Del Priore LV. Gene expression profile of cultured adult compared to immortalized human RPE. *Mol Vis.* 2006;12:1–14.
36. Tian J, Ishibashi K, Ishibashi K, et al. Advanced glycation endproduct-induced aging of the retinal pigment epithelium and choroid: a comprehensive transcriptional response. *Proc Natl Acad Sci U S A.* 2005;102:11846–11851.
37. Wang XF, Cui JZ, Nie W, Prasad SS, Matsubara JA. Differential gene expression of early and late passage retinal pigment epithelial cells. *Exp Eye Res.* 2004;79:209–221.
38. Weigel AL, Handa JT, Hjelmeland LM. Microarray analysis of H2O2-, HNE-, or tBH-treated ARPE-19 cells. *Free Radic Biol Med.* 2002;33:1419–1432.
39. Honda S, Farboud B, Hjelmeland LM, Handa JT. Induction of an aging mRNA retinal pigment epithelial cell phenotype by matrix-containing advanced glycation end products in vitro. *Invest Ophthalmol Vis Sci.* 2001;42:2419–2425.
40. Hollborn M, Stathopoulos C, Steffen A, Wiedemann P, Kohen L, Bringmann A. Positive feedback regulation between MMP-9 and VEGF in human RPE cells. *Invest Ophthalmol Vis Sci.* 2007;48: 4360–4367.
41. Leu ST, Batni S, Radeke MJ, Johnson LV, Anderson DH, Clegg DO. Drusen are cold spots for proteolysis: expression of matrix metalloproteinases and their tissue inhibitor proteins in age-related macular degeneration. *Exp Eye Res.* 2002;74:141–154.
42. Singh S, Zheng JJ, Peiper SC, McLaughlin BJ. Gene expression profile of ARPE-19 during repair of the monolayer. *Graefes Arch Clin Exp Ophthalmol.* 2001;239:946–951.
43. Lu H, Hunt DM, Ganti R, et al. Metallothionein protects retinal pigment epithelial cells against apoptosis and oxidative stress. *Exp Eye Res.* 2002;74:83–92.
44. Rollin R, Mediero A, Roldan-Pallares M, Fernandez-Cruz A, Fernandez-Durango R. Natriuretic peptide system in the human retina. *Mol Vis.* 2004;10:15–22.
45. Obata H, Kaburaki T, Kato M, Yamashita H. Expression of TGF-beta type I and type II receptors in rat eyes. *Curr Eye Res.* 1996;15: 335–340.
46. Rodriguez-Manas L, Sanchez-Rodriguez C, Vallejo S, et al. Pro-inflammatory effects of early non-enzymatic glycated proteins in human mesothelial cells vary with cell donor's age. *Br J Pharmacol.* 2006;149:979–987.
47. Yamagishi S, Okamoto T, Amano S, et al. Palmitate-induced apoptosis of microvascular endothelial cells and pericytes. *Mol Med.* 2002;8:179–184.

48. Schuster VL, Lu R, Coca-Prados M. The prostaglandin transporter is widely expressed in ocular tissues. *Surv Ophthalmol.* 1997; 41(suppl 2):S41–S45.
49. Garg TK, Chang JY. 15-Deoxy-delta 12, 14-prostaglandin J2 prevents reactive oxygen species generation and mitochondrial membrane depolarization induced by oxidative stress. *BMC Pharmacol.* 2004;4:6.
50. Yim MB, Yim HS, Lee C, Kang SO, Chock PB. Protein glycation: creation of catalytic sites for free radical generation. *Ann NY Acad Sci.* 2001;928:48–53.
51. Scivittaro V, Ganz MB, Weiss MF. AGEs induce oxidative stress and activate protein kinase C-beta(II) in neonatal mesangial cells. *Am J Physiol Renal Physiol.* 2000;278:F676–683.
52. Alizadeh M, Miyamura N, Handa JT, Hjelmeland LM. Human RPE cells express the FGFR2IIIc and FGFR3IIIc splice variants and FGF9 as a potential high affinity ligand. *Exp Eye Res.* 2003;76:249–256.
53. Alizadeh P, Smit-McBride Z, Oltjen SL, Hjelmeland LM. Regulation of cysteine cathepsin expression by oxidative stress in the retinal pigment epithelium/choroid of the mouse. *Exp Eye Res.* 2006;83: 679–687.
54. Zareba M, Raciti MW, Henry MM, Sarna T, Burke JM. Oxidative stress in ARPE-19 cultures: do melanosomes confer cytoprotection? *Free Radic Biol Med.* 2006;1;40(1):87–100.
55. Różanowski BK, Burke JM, Boulton ME, Sarna T, Rózanowska MB. Human RPE melanosomes protect from photosensitized and iron-mediated oxidation but become pro-oxidant in the presence of iron upon photodegradation. *Invest Ophthalmol Vis Sci.* 2008; 49(7):2838–2847.
56. Różanowski B, Cuenco J, Davies S, et al. The phototoxicity of aged human retinal melanosomes. *Photochem Photobiol.* 2008;84(3): 650–657.
57. Rózanowska M, Korytowski W, Różanowski B, et al. Photoreactivity of aged human RPE melanosomes: a comparison with lipofuscin. *Invest Ophthalmol Vis Sci.* 2002;43(7):2088–2096.
58. Yan SD, Schmidt AM, Anderson GM, et al. Enhanced cellular oxidant stress by the interaction of advanced glycation end products with their receptors/binding proteins. *J Biol Chem.* 1994;269: 9889–9897.
59. Hammes HP, Hoerauf H, Alt A, et al. N(epsilon)(carboxymethyl)lysin and the AGE receptor RAGE colocalize in age-related macular degeneration. *Invest Ophthalmol Vis Sci.* 1999;40:1855–1859.
60. Boulton M, Moriarty P, Jarvis-Evans J, Marcyniuk B. Regional variation and age-related changes of lysosomal enzymes in the human retinal pigment epithelium. *Br J Ophthalmol.* 1994;78:125–129.
61. Cingle KA, Kalski RS, Bruner WE, O'Brien CM, Erhard P, Wyszynski RE. Age-related changes of glycosidases in human retinal pigment epithelium. *Curr Eye Res.* 1996;15:433–438.
62. Hjelmeland LM, Cristofolo VJ, Funk W, Rakoczy E, Katz ML. Senescence of the retinal pigment epithelium. *Mol Vis.* 1999;5:33.
63. Shamsi FA, Boulton M. Inhibition of RPE lysosomal and antioxidant activity by the age pigment lipofuscin. *Invest Ophthalmol Vis Sci.* 2001;42:3041–3046.
64. Reckelhoff JF, Tygart VL, Mitias MM, Walcott JL. STZ-induced diabetes results in decreased activity of glomerular cathepsin and metalloprotease in rats. *Diabetes.* 1993;42:1425–1432.
65. Sebekova K, Schinzel R, Ling H, et al. Advanced glycated albumin impairs protein degradation in the kidney proximal tubules cell line LLC-PK1. *Cell Mol Biol* (*Noisy-le-grand*). 1998;44:1051–1060.
66. Kaemmerer E, Schutt F, Krohne TU, Holz FG, Kopitz J. Effects of lipid peroxidation-related protein modifications on RPE lysosomal functions and POS phagocytosis. *Invest Ophthalmol Vis Sci.* 2007; 48:1342–1347.
67. Rakoczy PE, Baines M, Kennedy CJ, Constable IJ. Correlation between autofluorescent debris accumulation and the presence of partially processed forms of cathepsin D in cultured retinal pigment epithelial cells challenged with rod outer segments. *Exp Eye Res.* 1996;63(2):159–167.
68. Rakoczy PE, Sarks SH, Daw N, Constable IJ. Distribution of cathepsin D in human eyes with or without age-related maculopathy. *Exp Eye Res.* 1999;69(4):367–374.